

We are IntechOpen, the world's leading publisher of Open Access books Built by scientists, for scientists

6,900

Open access books available

186,000

International authors and editors

200M

Downloads

Our authors are among the

154

Countries delivered to

TOP 1%

most cited scientists

12.2%

Contributors from top 500 universities



WEB OF SCIENCE™

Selection of our books indexed in the Book Citation Index
in Web of Science™ Core Collection (BKCI)

Interested in publishing with us?
Contact book.department@intechopen.com

Numbers displayed above are based on latest data collected.
For more information visit www.intechopen.com



Rotors on Active Magnetic Bearings: Modeling and Control Techniques

Andrea Tonoli, Angelo Bonfitto, Mario Silvagni and
Lester D. Suarez

Additional information is available at the end of the chapter

<http://dx.doi.org/10.5772/51298>

1. Introduction

In the last decades the deeper and more detailed understanding of rotating machinery dynamic behavior facilitated the study and the design of several devices aiming at friction reduction, vibration damping and control, rotational speed increase and mechanical design optimization. Among these devices a promising technology is represented by magnetic actuators used as bearings which found a great spread in rotordynamics and in high precision applications. A first classification of magnetic bearings according to the physical working principle allows to pick out two main families: a) Active Magnetic Bearings [1], [2], making use of an electronic control unit to regulate the current flowing in the coils of the actuators. They need external source of energy. b) Passive Magnetic Bearings [3], [4], [5]: they do not need any electronic equipment. The control of the mechanical structure is achieved without the introduction of any external energy source. They exploit the reluctance force or the Lorentz force due to the generation of eddy currents developed in a conductor in a relative motion in a magnetic field. Active Magnetic Bearings require sensors and electronic equipment but, although more expensive respect to classical ball bearings, they offer several technological advantages:

- The absence of all fatigue and tribology issues due to contact: it allows the use of such bearings in vacuum systems, in clean and sterile rooms, or for the transport of aggressive or very pure media, and at high temperatures;
- No lubrication needed;
- No contamination by the dust created by friction between the rotor and the stator;
- Low bearing losses: at high operating speeds are 5 to 20 times less than in conventional ball or journal bearings, result in lower operating costs;

- Viscous friction can be avoided if the rotor is confined in high vacuum;
- Low vibration level;
- Dynamics adaptable to the desired application by tuning of the control loop;
- Precise positioning of the rotor due to the control loop: this is mainly determined by the quality of the measurement signal within the control loop. Conventional inductive sensors, for example, have a measurement resolution of about $1 \div 1000 \mu\text{m}$ of a millimeter;
- Achievable fast positioning and/or high rotational speed of the rotor;
- The small sensitivity to the operating conditions;
- The predictability of the behavior.
- Further statements about the technology of realization can be done:
 - The gap between rotor and bearing amounts typically to a few tenths of a millimeter, but for specific applications it can be as large as 20 mm. In that case, of course, the bearing becomes much larger;
 - The rotor can be allowed to rotate at high speeds. The high circumferential speed in the bearing, only limited by the strength of material of the rotor, offers the possibilities of designing new machines with higher power density and of realizing novel constructions. Actually, about 350 m/s are achievable, for example by using amorphous metals which can sustain high stresses and at the same time have very good soft-magnetic properties, or by binding the rotor laminations with carbon fibers. Design advantages result from the absence of lubrication seals and from the possibility of having a higher shaft diameter at the bearing site. This makes the shaft stiffer and less sensitive to vibrations;
 - The specific load capacity of the bearing depends on the type of ferromagnetic material and the design of the bearing electromagnet. It will be about 20 N/cm² and can be as high as 40 N/cm². The reference area is the cross sectional area of the bearing. Thus the maximum bearing load is mainly a function of the bearing size;
 - The bearing and the rotor can be integrated on the same shaft by realizing bearingless configurations which allow to reduce the size of the system and to perform a cost saving solution.
 - Retainer bearings are additional ball or journal bearings, which in normal operation are not in contact with the rotor. In case of overload or malfunction of the AMB they have to operate for a very short time: they keep the spinning rotor from touching the housing until the rotor comes to rest or until the AMB regains control of the rotor. The design of such retainer bearings depends on the specific application and despite a variety of good solutions still needs special attention;
 - The unbalance compensation and the force-free rotation are control features where the vibrations due to residual unbalance are measured and identified by the AMB. The signal is used to either generate counteracting and compensating bearing forces or to shift the rotor axis in such a way that the rotor is rotating force-free;

- Diagnostics are readily performed, as the states of the rotor are measured for the operation of the AMB anyway, and this information can be used to check operating conditions and performance. Even active diagnostics are feasible, by using the AMB as actuators for generating well defined test signals simultaneously with their bearing function;
- The lower maintenance costs and higher life time of an AMB have been demonstrated under severe conditions. Essentially, they are due to the lack of mechanical wear. Currently, this is the main reason for the increasing number of applications in turbomachinery;
- The cost structure of an AMB is that of a typical mechatronics product. The costs for developing a prototype, mainly because of the demanding software, can be rather high. On the other side, a series production will lower the costs considerably because of the portability of that software.

Active Magnetic Bearings can be classified as a typical mechatronic product due to its nature which involves mechanical, electrical and control aspects, merging them in a single system. Rotordynamic field offer several examples of application areas [1], [6] : (a) Turbomachinery, (b) Vibration isolation, (c) Machine tools and electric drives, (d) Energy storing flywheels, (e) Instruments in space and physics, (f) Non-contacting suspensions for micro-techniques, (g) Identification and test equipment in rotordynamics, (f) Microapplications such as gyroscopic sensors [7], [8]. The attractive potential of active magnetic suspensions motivated a considerable research effort for the past decade focused mostly on electrical actuation subsystem and control strategies [3], [9], [10], [11], [12], [13], [14].

This chapter illustrates the design, the modeling, the experimental tests and validation of all subsystems of a rotor on a five-axes active magnetic suspension. The mechanical, electrical, electronic and control strategies aspects are explained with a mechatronic approach evaluating all the interactions between them. The main goals of the manuscript are: a) Illustrate the design and the modeling phases of a five-axes active magnetic suspension; b) Discuss the design steps and the practical implementation of a standard suspension control strategy; c) Introduce an off-line technique of electrical centering of the actuators. The experimental test rig is a shaft (Weight: 5.3 kg. Length: 0.5 m) supported by two radial and one axial cylindrical active magnetic bearings and powered by an asynchronous high frequency electric motor. The chapter starts on an overview of the most common technologies used to support rotors with a deep analysis of their advantages and drawbacks with respect to active magnetic bearings. Furthermore a discussion on magnetic suspensions state of the art is carried out highlighting the research efforts directions and the goals reached in the last years. In the central sections, a detailed description of each subsystem is performed along with the modeling steps. In particular the rotor is modeled with a FE code while the actuators are considered in a linearized model.

The last sections of the chapter are focused on the control strategies design and the experimental tests. An off-line technique of actuators electrical centering is explained and its advantages are described in the control design context. This strategy can be summarized as follows. Knowing that: a) each actuation axis is composed by two electromagnets; b) each electromagnet needs a current closed-loop control; c) the bandwidth of this control is depending on the mechanical Airgap, then the technique allows obtaining the same value of

the closed-loop bandwidth of the current control of both the electromagnets on the same actuation axis. This approach improves performance and gives more steadiness to the control behavior. The decentralized approach of the control strategy allowing the full suspensions on five axes is illustrated from the design steps to the practical implementation on the control unit. Finally, the experimental tests are carried out on the rotor to validate the suspension control and the off-line electrical centering. The numerical and experimental results are superimposed and compared to prove the effectiveness of the modeling approach.

2. System Architecture

The rig used for the modeling, the design and the experimental tests is an electrical spindle (picture reported in Figure 1) consisting of a shaft supported by two radial and one axial active magnetic bearings with cylindrical geometry and powered by an asynchronous high frequency electric motor. Two mechanical ball bearings, with radial and axial airgaps equal to half of the levitation ones, are positioned at the ends of the shaft to guarantee a safely touch-down of the shaft for anomalous working conditions with excessive whirling amplitude. The rotation axis is horizontal and the weight has the direction of each bearing.

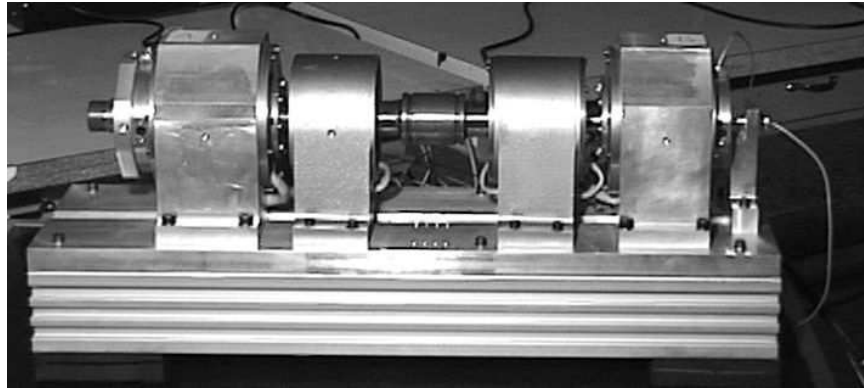


Figure 1. Picture of the rotor.

Parameter	Symbol	Value	Unit
Rotor mass	m	5.31	kg
Rotor transversal Inertia	$J_x=J_y$	$1.153 \cdot 10^{-1}$	Kg/m ²
Rotor polar Inertia	J_z	$1.826 \cdot 10^{-3}$	Kg/m ²
Bearing rad. 1 location	a	214.5	mm A/V
Bearing rad. 2 location	b	212.6	mm A/V
Axial/Radial Airgap	g	$0.75e-3$	mm
Isotropic support stiffness	f / x	$2.5 \cdot 10^{-5}$	N/m

Table 1. Rotor mechanical and geometric parameters.

Table 1 reports the main parameters of the rotor. Figure 2 illustrates the section view of the system showing the layout of sensors, actuators, motor and rotor.

Active Magnetic Bearings applied to rotating machines can be considered as a typical mechatronic application, since it involves the control of mechanical system (the rotor) by means of an electronic control unit which elaborates the commands to feed electrical power drivers regulating the electromechanical actuators. The information to perform closed loop control architecture is given by displacement and current sensors.

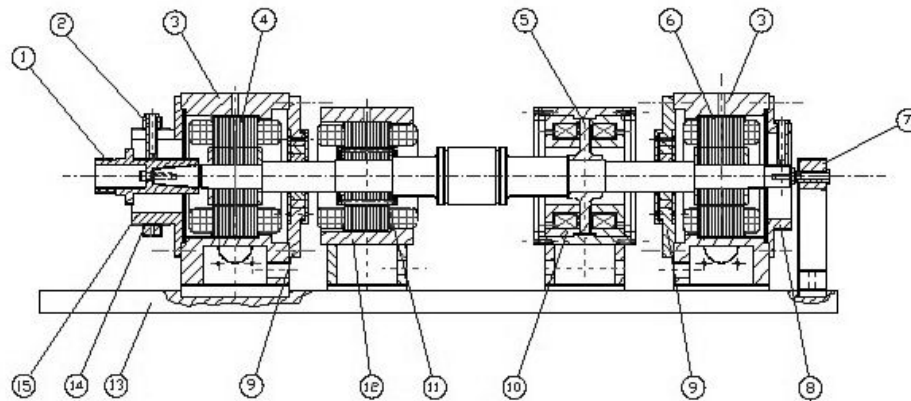


Figure 2. System section view: 1) tang, 2) radial sensor, 3) radial AMB support, 4) radial AMB laminated stator, 5) axial AMB disc, 6) radial AMB laminated stator, 7) axial sensor, 8) sensor cap, 9) bushing cap, 10) axial AMB electromagnet, 11) electric motor, 12) motor support, 13) foundation, 14) threaded ring, 15) sensor cap.

The interactions and the main functions of these subsystems are highlighted in Figure 3. The reported scheme is a standard representation of the system. However each block can be of different nature depending on the application. A short summary of the technologies typically used for each subsystem and the technologies used in the rig described in this chapter are reported in the following sections.

2.1. Control

Two main families of control architecture can be listed for active magnetic bearings:

- Decentralized SISO control: the action of each actuator is independent from the others and exploits a dedicated control law and sensors information;
- Centralized MIMO control: actuators are coupled as well as sensors information. A single control action is devoted to feed power drivers.

Several control strategies have been implemented and tested on rotors equipped with active magnetic bearings:

- Gain scheduled control [15];
- Adaptive control [16], [17];

- Robust H^∞ control [18];
- Robust sliding mode control [19];
- Robust control via eigenstructure assignment dynamical compensation [20];
- Optimal control [21];
- Dynamic programming control [22];
- Genetic algorithm control [23];
- Fuzzy logic control [24];
- Feedback linearization control [25];
- Time-delay control [26];
- Control by transfer function approach [27];
- μ -synthesis control [28].

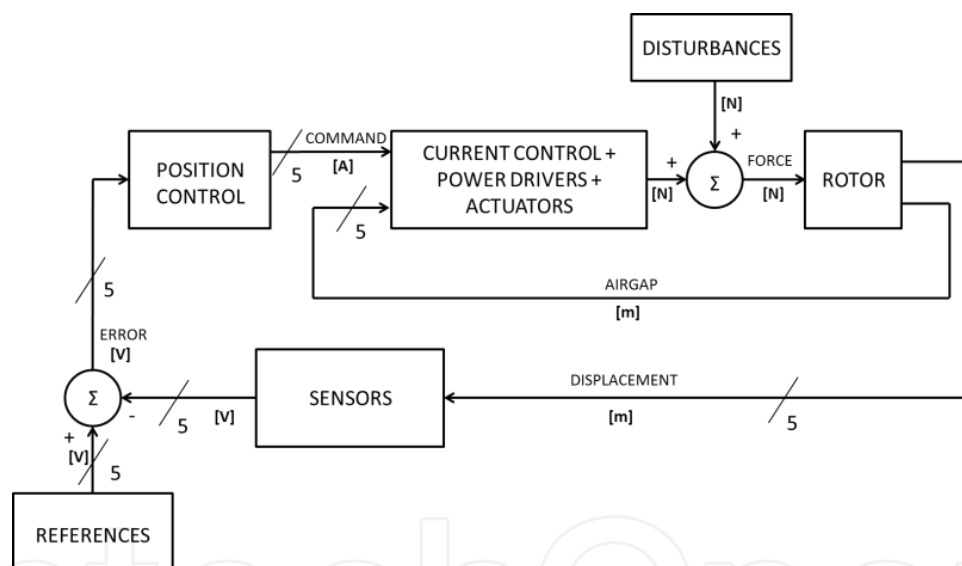


Figure 3. Overall system architecture.

In this chapter a decentralized PID strategy is implemented on a control module equipped with a DSP/FPGA-based digital control unit (EKU2.1). This digital platform allows the rapid reconfigurations of the overall system through up to 108 (from FPGA) and 46 (from DSP) configurable digital I/O lines for input/output, event, PWM, capture/generation and user functions. Both DSP and FPGA have a dedicated Hard Real-Time Operating System (HRTOS) based on a non-pre-emptive scheduler (DSP side), involving ISR time or event triggered. EKU2.1 uses a single-master (DSP) multi-slave (FPGA) point-to-point communication protocol, based on Wishbone format; a system bus manages data exchange between the two cores. Software code is developed using the target-dependent tools Texas Instruments® Code Composer Studio.

2.2. Power drivers

The electronic circuits of power amplification stage to convert low power controller output signal to a high power stator input signal is chosen according to the kind of application. Basically, three main families of electronic circuits can be identified:

1. Linear analogue amplifiers have push–pull transistors at the output stage. They allow to enhance the current capability and to integrate a high-gain linear amplifier, such as a power operational amplifier. The linear amplifiers have the advantage of precise current and voltage regulation as well as low noise and they have a current rating of less than 10 A. Operation at the rated current is available only with effective cooling with heat sinks. Therefore the amplifier dimensions are large, resulting in high cost. The efficiency is low because of high losses in the push–pull transistor.
2. Switched-mode amplifiers enhance efficiency. Since the losses in the power devices are reduced, the heat sinks are much smaller and, as a result, switched mode amplifiers are compact in dimension so that the cost is low. Switched-mode operation of power devices is widely used in industry, e.g., for general-purpose inverters in ac drives and computer power supplies. This category of amplifiers is dominant in magnetic bearing drivers.

Hybrid amplifiers take advantage of linear and switched-mode amplifiers. At low current the push–pull transistors operate as a linear amplifier but at high current they operate in switched mode. To take advantage of a hybrid amplifier, it is quite important to modify the winding structure in magnetic bearings.

The rig object of study in this chapter is equipped with an H-bridge switching amplifier for each actuator. The power stage consists of an Embedded Isolated Power Module Board with four fully independent MOSFET/IGBT legs that supports up to 25 amperes with 100 volt of DC Bus. Also a maximum PWM switching frequency is 80kHz making this module suitable for high performance driving applications where control loop bandwidth and current ripple are important factors. The scheme used to feed power drivers is reported in Figure 4.

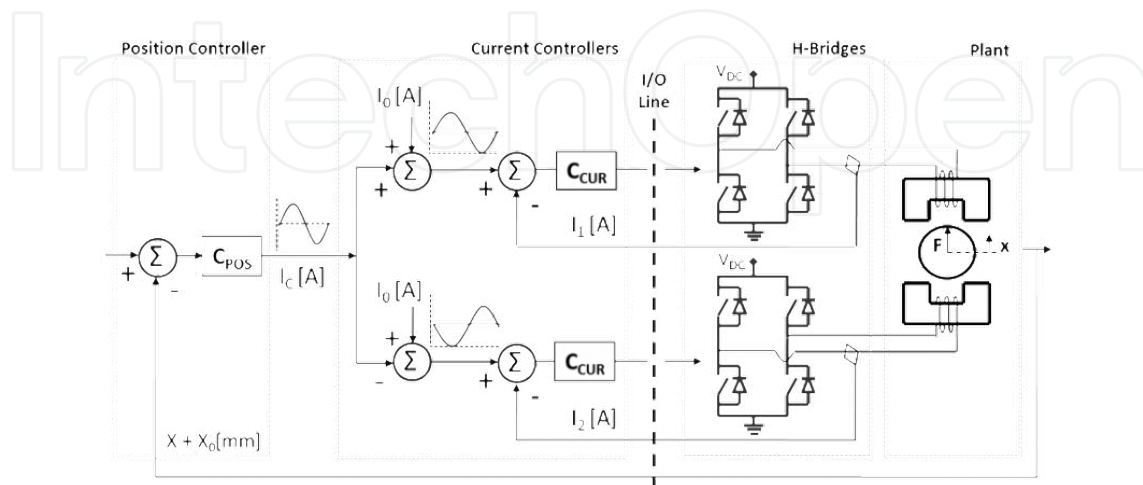


Figure 4. Power driver scheme.

Standard AMBs equipment for rotors suspensions are realized with five couples of cylindrical shape electromagnets to perform five dof active control. Conical shape of magnetic bearings exerting forces both in axial and radial direction simultaneously allow to save one couple of electromagnets and hence to reduce the size although the bearing design results more complex than standard cylindrical solution. This geometry permits to reach higher rotation speed, limited in cylindrical solution by the strains growing in axial bearing disc.

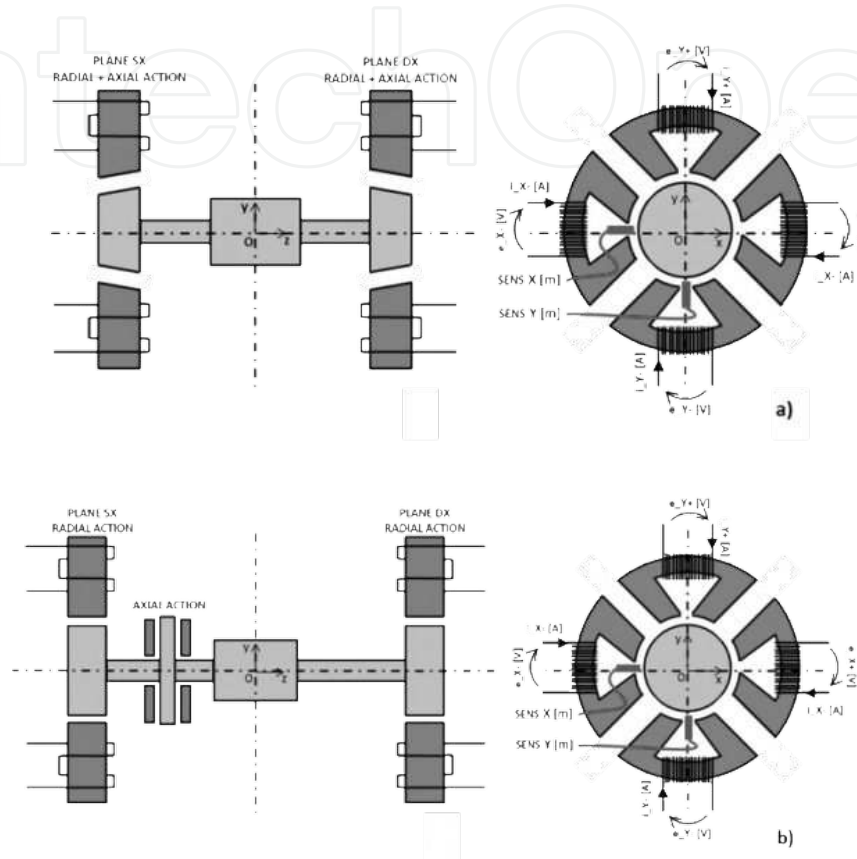


Figure 5. Geometry of actuation stage. a) Conical profile. b) Cylindrical profile.

2.3. Actuators

Actuators geometry and configuration depends on the electromagnets profile and on the number of actuators per actuation stage.

In this work classical configuration with four cylindrical actuators per actuation stage is dealt with. The disposition of the ten electromagnets is illustrated in Figure 6.

The main electrical and geometrical actuators parameters are listed in Table 2.

Parameter	Symbol	Value	Unit
Vacuum permeability	μ_0	1.26e-006	H/m
Voltage supply	V_{DC}	50	V

Parameter	Symbol	Value	Unit
AXIAL Actuator			
Number of turns	N_{AX}	120	-
Circuitation length	l_{AX}	48e-3	m
Active section on airgap	S_{AX}	1210e-6	m ²
Nominal airgap	$g_{0_{AX}}$	0.75e-3	m
Resistance	R_{AX}	0.5	Ω
Nominal inductance	$L_{0_{AX}}$	0.0146	H
RADIAL actuator			
Number of turns	N_{RAD}	110	-
Circuitation length	l_{RAD}	135.2e-3	m
Active section on airgap	S_{RAD}	480e-6	m ²
Nominal airgap	$g_{0_{RAD}}$	0.75e-3	M
Resistance	R_{RAD}	0.5	Ω
Nominal Inductance	$L_{0_{RAD}}$	0.0049	H

Table 2. Actuators parameters.

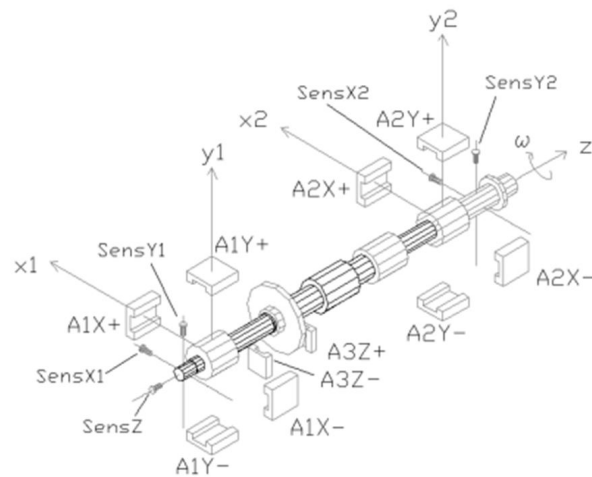


Figure 6. Actuators configuration.

2.4. Sensors

An important part of the performance of a magnetic bearing depends on the characteristics of the displacement sensors used. In order to measure the position of a moving rotor, contact-free sensors must be used which, moreover, must be able to measure on a rotating sur-

face. Consequently, the geometry of the rotor, i.e. its surface quality, and the homogeneity of the material at the sensor will also influence the measuring results. A bad surface will thus produce noise disturbances, and geometry errors may cause disturbances with the rotational frequency or with multiples thereof.

In addition, depending on the application, speeds, currents, flux densities and temperatures are to be measured in magnetic bearing systems.

When selecting the displacement sensors, depending on the application of the magnetic bearing, measuring range, linearity, sensitivity, resolution, and frequency range are to be taken into account as well as:

- Temperature range, temperature drift of the zero point and sensitivity;
- Noise immunity against other sensors, magnetic alternating fields of the electromagnets, electromagnetic disturbances from switched amplifiers;
- Environmental factors such as dust, aggressive media, vacuum, or radiation;
- Mechanical factors such as shock and vibration;
- Electrical factors such as grounding issues associated with capacitive sensors.

The most important displacement sensors technologies are:

- Inductive sensors;
- Eddy-current sensors;
- Eddy Current Radial Displacement Sensor on a PCB (Transverse Flux Sensor)
- Capacitive sensors;
- Magnetic sensors.

The rig described in this chapter is equipped with five eddy current displacement sensors: high-frequency alternating current runs through the air-coil embedded in a housing. The electromagnetic coil section induces eddy currents in the conductive object whose position is to be measured, thus absorbing energy from the oscillating circuit. Depending on the clearance, the inductance of the coil varies, and external electronic circuitry converts this variation into an output signal. The usual modulation frequencies lie in a range of 1 - 2 MHz, resulting in useful measuring frequency ranges of 0 Hz up to approximately 20 kHz.

3. Modeling

The dynamic behavior of the rotor can be described by means of different models. This section describes the modeling techniques and the adopted assumptions, how acting forces and displacements are ordered and selected, the equation of motion used for the dynamic description and the variable used to describe the models.

Many modeling techniques can be adopted; an analytical rigid approach (based on the 4 d.o.f. rotor modeling) is here presented beside the most common Finite Element (FE) approach. The discretization for FEM software is reported in Figure 7.b.

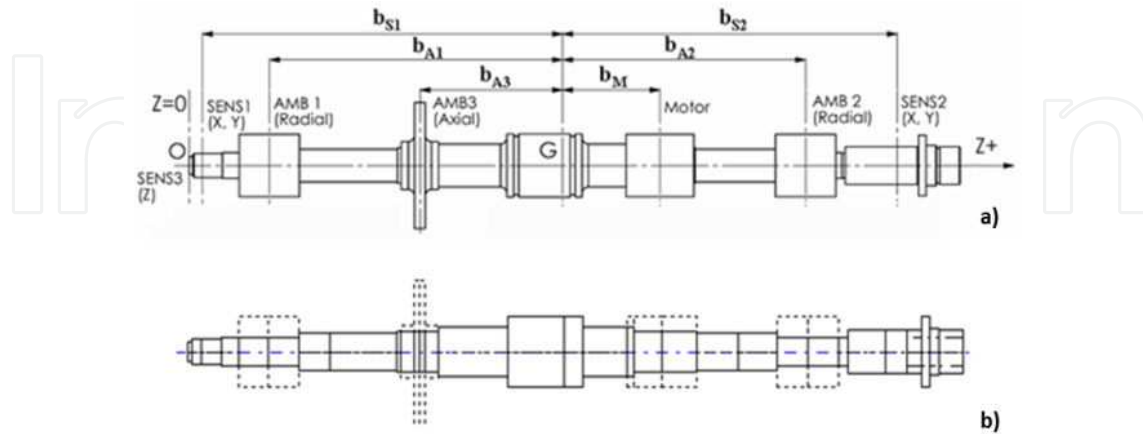


Figure 7. Rotor section view. a) View with dimensions. b) Discretization for FEM modeling.

The main hypothesis here adopted is to consider a constant spin speed. In this case the rotor behavior on the X-Y plane (known as flexural) is not coupled with the behavior on the Z-direction (axial). Other important assumption is that any rotation (except for spinning rotation) should be small.

3.1. Model Block Diagram

A simple description of the rotor model block diagram is presented in Figure 8. Forces (due to AMBs, motor and external) acting on the rotor are un-grouped for the X-Y and for the Z behavior, these signals are fed to the block describing the dynamic behaviors. Outputs of these blocks are the states (displacements and velocities) of the systems, reported as displacements and speeds to sensors, AMBs and motor. The constant spin speed Ω is used in the X-Y model for the gyroscopic behavior and reported as output. Spin speed and displacement on the sensors are physical entities measured by specific sensors, and signal are reported to the Sensor block; the other displacements and relative velocities (to AMBs and motor) should be used for intrinsic feedback such as back electro-motive force in the motor or magnetic bearings.

3.1.1. Model inputs / outputs

Model inputs are the forces acting on the rotor, while outputs are typically displacements either on sensors or on AMBs and motor (Figure 9). The rotor is suspended by two radial magnetic bearing (AMB1 and AMB2) which generate four forces oriented as the reference plant reference frame and acting in the center of the relative AMB; these forces act the behavior on X-Y plane. A further magnetic bearing (AMB3) is used to constrain displacements along Z axis (axial). The five forces due to AMBs are collected in vector f_{AMB} . The electric

motor, used to generate rotation torque (not included in this kind of model where the spin speed is assumed to be constant), can also act two forces, in radial direction, while is not capable to generate a force in the Z direction. According to this, vector f_{MOT} has two components acting in the center of the motor.

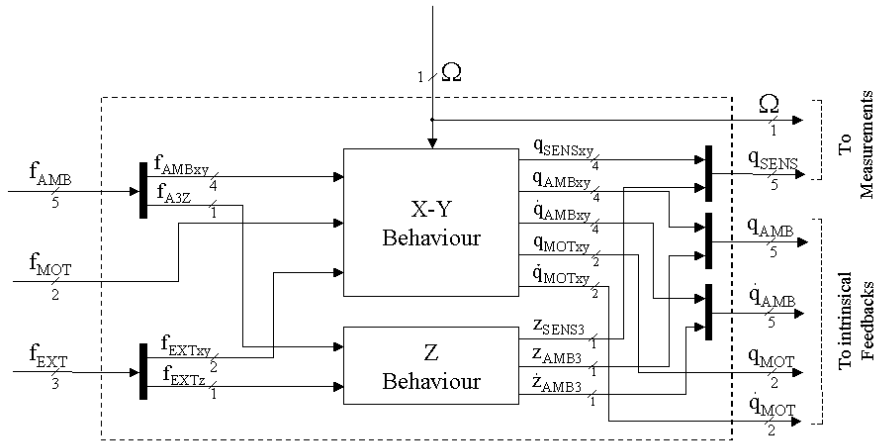


Figure 8. Rotor model block diagram.

In order to simplify the description of the system the generic external force are supposed to act directly to the center of mass of the rotor; these three forces are oriented as the plant reference frame. These components are the resultant of any external force, such as impact forces. While the X-Y behaviour is uncoupled from the Z behavior, acting forces due to AMBs and external can be rewritten dividing the forces acting in X-Y plane from forces acting on Z axis. Table 3 reports acting forces (inputs) on the rotor.

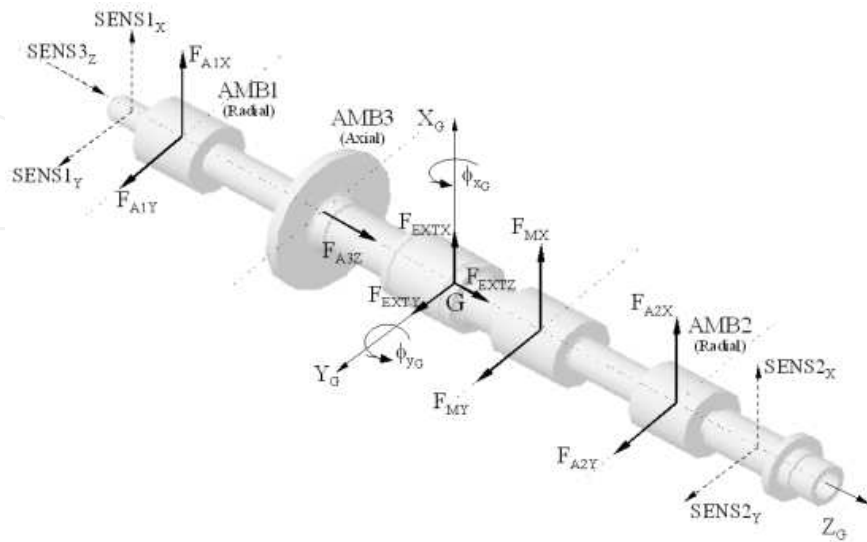


Figure 9. Actuation forces and sensors position.

AMB	Motor	External
$\mathbf{f}_{AMB} = \begin{Bmatrix} F_{A1X} \\ F_{A1Y} \\ F_{A2X} \\ F_{A2Y} \\ F_{A3Z} \end{Bmatrix} = \begin{Bmatrix} \mathbf{f}_{AMBxy} \\ F_{A3Z} \end{Bmatrix}$	$\mathbf{f}_{MOT} = \begin{Bmatrix} F_{MX} \\ F_{MY} \end{Bmatrix}$	$\mathbf{f}_{EXT} = \begin{Bmatrix} F_{EXTx} \\ F_{EXTy} \\ F_{EXTz} \end{Bmatrix} = \begin{Bmatrix} \mathbf{f}_{EXTxy} \\ F_{EXTz} \end{Bmatrix}$

(1)

Table 3. Rotor Inputs.

Referring to Figure 8, a set of outputs is used for measurements (the spin speed Ω and the displacements on the sensor q_{SENS}) and another set is used for intrinsic feedback (displacements and velocities on AMBs q_{AMB} and \dot{q}_{AMB} , and on the motor q_{MOT} and \dot{q}_{MOT}).

Table 4 reports displacements and velocities (outputs) on the rotor.

Sensors	AMB	Motor
$\mathbf{q}_{SENS} = \begin{Bmatrix} x_{SENS1} \\ y_{SENS1} \\ x_{SENS2} \\ y_{SENS2} \\ z_{SENS3} \end{Bmatrix} = \begin{Bmatrix} \mathbf{q}_{SENSxy} \\ z_{SENS3} \end{Bmatrix}$	$\mathbf{q}_{AMB} = \begin{Bmatrix} x_{AMB1} \\ y_{AMB1} \\ x_{AMB2} \\ y_{AMB2} \\ z_{AMB3} \end{Bmatrix} = \begin{Bmatrix} \mathbf{q}_{AMBxy} \\ z_{AMB3} \end{Bmatrix}$	$\mathbf{q}_{MOT} = \begin{Bmatrix} x_{MOT} \\ y_{MOT} \\ z_{MOT} \end{Bmatrix}$

(2)

Table 4. Rotor outputs.

Input		Output	
X-Y Behaviour	Z Behaviour	X-Y Behaviour	Z Behaviour
$\mathbf{f}_{xy} = \begin{Bmatrix} F_{A1X} \\ F_{EXTx} \\ F_{MX} \\ F_{A2X} \\ F_{A1Y} \\ F_{EXTx} \\ F_{MY} \\ F_{A2Y} \end{Bmatrix}$	$\mathbf{f}_z = \begin{Bmatrix} F_{A3Z} \\ F_{EXTz} \end{Bmatrix}$	$\mathbf{y}_{xy} = \begin{Bmatrix} x_{SENS1} \\ x_{AMB1} \\ x_{MOT} \\ x_{AMB2} \\ x_{SENS2} \\ y_{SENS1} \\ y_{AMB1} \\ y_{MOT} \\ y_{AMB2} \\ y_{SENS2} \end{Bmatrix}$	$\mathbf{y}_z = \begin{Bmatrix} z_{SENS3} \\ z_{AMB3} \end{Bmatrix}$

(3)

Table 5. Inputs / Outputs vector orders.

Input/Output vector reported in Table 5. and ordered to be compliant with blocks that generate such forces. In order to address the modeling technique (especially FE based), input/output vector should be reordered in the way reported in Table 5.

The dynamic behavior of the rotor can be described by mean of the equations of motion (EoM). In the following section the equations used for the model is described. The typical equations are reported for a generic rotor model and then applied to a rigid analytical model and to the FE model. While the spin speed is constant the X-Y behavior is uncoupled from Z behavior in the same way the equations can be separated.

X-Y Behavior

Equation of Motion:

$$\begin{aligned} \mathbf{M}_{xy} \ddot{\mathbf{q}}_{xy}(t) + (\mathbf{L}_{xy} + \Omega \mathbf{G}_{xy}) \dot{\mathbf{q}}_{xy}(t) + (\mathbf{K}_{\Omega 0xy} + \Omega^2 \mathbf{K}_{\Omega 2xy} + \Omega \mathbf{H}_{xy}) \mathbf{q}_{xy}(t) = \\ = \mathbf{f}_{sxy} + \Omega^2 \mathbf{f}_{umb} \begin{Bmatrix} \sin(\Omega t) \\ \cos(\Omega t) \end{Bmatrix} + \mathbf{S}_{ixy} \mathbf{f}_{xy}(t) \end{aligned} \quad (1)$$

Measure Equation:

$$\begin{Bmatrix} \mathbf{y}_{xy}(t) \\ \dot{\mathbf{y}}_{xy}(t) \end{Bmatrix} = \mathbf{S}_{oxy} \begin{Bmatrix} \mathbf{q}_{xy}(t) \\ \dot{\mathbf{q}}_{xy}(t) \end{Bmatrix} \quad (2)$$

Z Behavior

Equation of Motion:

$$\mathbf{M}_z \ddot{\mathbf{q}}_z(t) + \mathbf{L}_z \dot{\mathbf{q}}_z(t) + (\mathbf{K}_{\Omega 0z} + \Omega^2 \mathbf{K}_{\Omega 2z}) \mathbf{q}_z(t) = \mathbf{f}_{sz} + \mathbf{S}_{iz} \mathbf{f}_z(t) \quad (3)$$

Measure Equation:

$$\begin{Bmatrix} \mathbf{y}_z(t) \\ \dot{\mathbf{y}}_z(t) \end{Bmatrix} = \mathbf{S}_{oz} \begin{Bmatrix} \mathbf{q}_z(t) \\ \dot{\mathbf{q}}_z(t) \end{Bmatrix} \quad (4)$$

Refer to Table 6 for matrices naming and description.

Name	Description
Ω	Spin Speed
$\mathbf{q}(t)$	Generalized displacements

Name	Description
M	Mass (symmetric) matrix
L	Damping (symmetric) matrix
G	Gyroscopic (skew-symmetric) matrix
$K_{\Omega 0}$	Stiffness (symmetric) matrix: spin speed independent
$K_{\Omega 2}$	Stiffness (symmetric) matrix: spin speed dependent
H	Circulatory (skew-symmetric) matrix
f_s	Static forces
R	Rotation Matrix
f_{umb}	Unbalance forces
$f(t)$	External forces
S_i	Input selection matrix
$y(t)$	Output displacements
S_o	Output selection matrix
Φ	Selected eigenvector for modal (MK) reduction

Table 6. Matrices names and description.

3.2. 4dof model

Generic Eom for rotors previously described, can be applied to a rigid analytical model based on the 4 d.o.f theory (for X-Y behavior), with an additional d.o.f. for the Z behavior. In this model the equation of motion are develop in a center of mass coordinate system as reported in Figure 10.

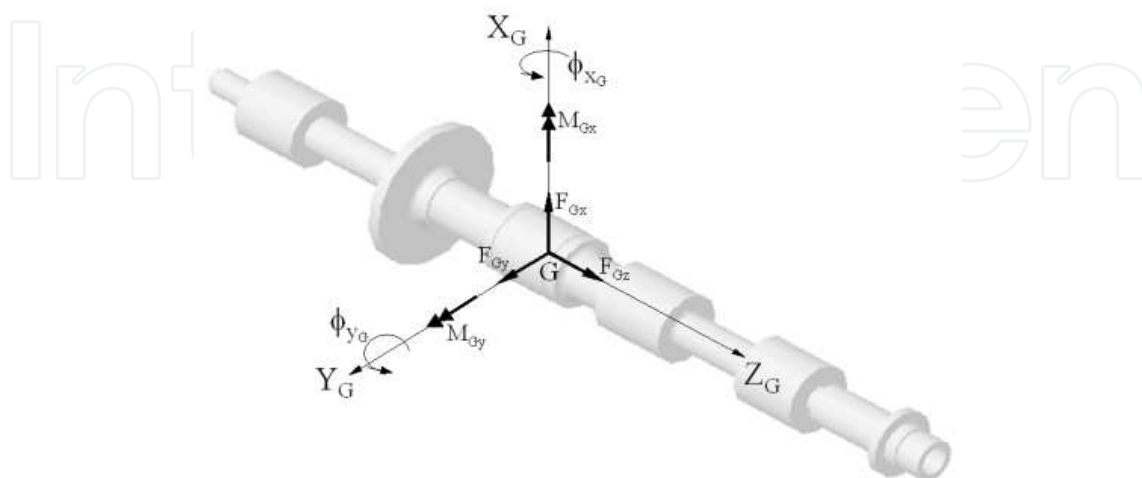


Figure 10. d.o.f. model with generalized displacements and forces.

The physical properties used in the model are:

Name	Description
m	Mass of the rotor [kg]
J_t	Transversal moment of inertia about any axis in the rotation plane [kgm ²]
J_p	Transversal moment of inertia about any axis in the rotation plane [kgm ²]
g_x, g_y	Gravity along x and y direction [m/s ²]
$\varepsilon_x, \varepsilon_y$	Static unbalance eccentricity along x and y direction [m]
χ	Torque unbalance: angular error [rad]
b_{A1}	AMB1 distance from center of mass [m]
b_{A2}	AMB2 distance from center of mass [m]
b_M	Motor distance from center of mass [m]
b_{S1}	Sensor1 distance from center of mass [m]
b_{S2}	Sensor2 distance from center of mass [m]

Table 7. Physical properties of rigid analytical model.

X-Y Behavior

The generalized displacements vector is composed by the center of mass coordinates:

$$\mathbf{q}_{xy}(t) = \begin{Bmatrix} x_G \\ y_G \\ \varphi_{x_G} \\ \varphi_{y_G} \end{Bmatrix} \quad (5)$$

If the model has no damping the EoM (4) becomes:

$$\begin{bmatrix} m & 0 & 0 & 0 \\ 0 & m & 0 & 0 \\ 0 & 0 & J_t & 0 \\ 0 & 0 & 0 & J_t \end{bmatrix} \ddot{\mathbf{q}}_{xy}(t) + \Omega \begin{bmatrix} 0 & 0 & 0 & 0 \\ 0 & 0 & 0 & 0 \\ 0 & 0 & 0 & J_p \\ 0 & 0 & -J_p & 0 \end{bmatrix} \dot{\mathbf{q}}_{xy}(t) = \begin{Bmatrix} mg_x \\ mg_y \\ 0 \\ 0 \end{Bmatrix} + \Omega^2 \begin{bmatrix} -m\varepsilon_y & m\varepsilon_x \\ m\varepsilon_x & m\varepsilon_y \\ -\chi(J_t - J_p) & 0 \\ 0 & \chi(J_t - J_p) \end{bmatrix} \begin{Bmatrix} \sin(\Omega t) \\ \cos(\Omega t) \end{Bmatrix} + \mathbf{S}_{ixy} \mathbf{f}_{xy}(t) \quad (6)$$

The measure equation has the same structure reported in (5).

Z Behavior

Under the same assumptions equation (6) becomes:

$$m\ddot{z}(t) = \mathbf{f}_{sz} + \mathbf{S}_{iz}\mathbf{f}_z(t) \tag{7}$$

The measure equation has the same structure reported in (7).

In order to be compliant to input/output vector described in Table 8 the selection matrices of equation (9) and (10) with their relative measure equation should be:

X-Y Behaviour	Z Behaviour
$\mathbf{S}_{ixy} = \begin{bmatrix} 1 & 1 & 1 & 1 & 0 & 0 & 0 & 0 \\ 0 & 0 & 0 & 0 & 1 & 1 & 1 & 1 \\ 0 & 0 & 0 & 0 & b_{A1} & 0 & -b_M & -b_{A2} \\ -b_{A1} & 0 & b_M & b_{A2} & 0 & 0 & 0 & 0 \end{bmatrix}_{4 \times 8}$	$\mathbf{S}_{iz} = \begin{bmatrix} 1 & 1 \end{bmatrix}_{1 \times 2}$
$\mathbf{S}_{oxy} = \begin{bmatrix} \mathbf{S}'_{oxy} & \mathbf{0} \\ \mathbf{0} & \mathbf{S}'_{oxy} \end{bmatrix}_{20 \times 8}, \mathbf{S}'_{oxy} = \begin{bmatrix} 1 & 0 & 0 & -b_{S1} \\ 1 & 0 & 0 & -b_{A1} \\ 1 & 0 & 0 & b_M \\ 1 & 0 & 0 & b_{A2} \\ 1 & 0 & 0 & b_{S2} \\ 0 & 1 & b_{S1} & 0 \\ 0 & 1 & b_{A1} & 0 \\ 0 & 1 & -b_M & 0 \\ 0 & 1 & -b_{A2} & 0 \\ 0 & 1 & -b_{S2} & 0 \end{bmatrix}$	$\mathbf{S}_{oz} = \begin{bmatrix} 1 & 0 \\ 1 & 0 \\ 0 & 1 \\ 0 & 1 \end{bmatrix}_{4 \times 2}$

Table 8. Input/Output selection matrices for rigid analytical model.

3.3. Flexible Rotor Model (FE)

A flexible model is here described. This model is generated by using a finite element code especially designed for rotating machines (Dynrot). The outputs of this code are the matrices reported in equation (4) to (7).

3.3.1. Full Model

In the case all the nodes displacements are used the full dynamic behavior is described. The displacements vector q collects the translation displacement of the model nodes in the following order:

3.3.1. Reduced Model

Usually a reduced model is used. A typical reduction method is the modal (MK) reduction where only some modes of vibration are selected.

The displacements to modal transformation are reported in Table 10:

X-Y Behaviour	Z Behaviour
$\mathbf{q}_{xy}(t) = \begin{Bmatrix} x_1 \\ x_2 \\ \dots \\ x_n \\ y_1 \\ y_2 \\ \dots \\ y_n \end{Bmatrix}$	$\mathbf{q}_z(t) = \begin{Bmatrix} z_1 \\ z_2 \\ \dots \\ z_n \end{Bmatrix}$

(12)

Table 9. Generalized coordinates for full FE model.

X-Y Behaviour	Z Behaviour
$\xi_{xy}(t) = \Phi_{xy} \mathbf{q}_{xy}(t)$	$\xi_z(t) = \Phi_z \mathbf{q}_z(t)$

(13)

Table 10. Nodal to Modal transformation.

The equations of motion for the reduced model are formerly the same reported in equations (4) to (7), where the nodal displacements is substituted by the modal displacements and matrices and vector are reported in their modal forms.

Input/output selection matrices should be transformed, starting from FEM matrices, as indicated in:

X-Y Behaviour	Z Behaviour
$\mathbf{S}_{\xi_{ixy}} = \Phi_{xy}^T \mathbf{S}_{ixy}$	$\mathbf{S}_{\xi_i} = \Phi_z^T \mathbf{S}_{iz}$
$\mathbf{S}_{\xi_{oxy}} = \mathbf{S}_{oxy} \Phi_{xy}$	$\mathbf{S}_{\xi_{oz}} = \mathbf{S}_{oz} \Phi_z$

(14)

Table 11. Input / Output matrices conversion from Nodal to Modal.

3.4. State Space representation of rotor dynamic equations

Dynamic equations (4) to (7) can be reported, with explicit spin speed, in the state space representation in the following way, either for X-Y or Z behavior:

$$\begin{aligned} \dot{\mathbf{x}}(t) &= (\mathbf{A}_{\Omega 0} + \Omega \mathbf{A}_{\Omega 1} + \Omega^2 \mathbf{A}_{\Omega 2}) \mathbf{x}(t) \mathbf{u}(t) + \mathbf{B} \mathbf{u}(t) \\ \mathbf{y}(t) &= \mathbf{C} \mathbf{x}(t) + \mathbf{D} \mathbf{u}(t) \end{aligned} \quad (8)$$

Where:

Name	X-Y Behaviour	Z Behaviour	(16)
$\mathbf{x}(t)$	$\begin{Bmatrix} \mathbf{q}_{xy}(t) \\ \dot{\mathbf{q}}_{xy}(t) \end{Bmatrix}$	$\begin{Bmatrix} \mathbf{q}_z(t) \\ \dot{\mathbf{q}}_z(t) \end{Bmatrix}$	
$\mathbf{A}_{\Omega 0}$	$\begin{bmatrix} \mathbf{0} & \mathbf{I} \\ -\mathbf{M}_{xy}^{-1} \mathbf{K}_{\Omega 0 xy} & -\mathbf{M}_{xy}^{-1} \mathbf{L}_{xy} \end{bmatrix}$	$\begin{bmatrix} \mathbf{0} & \mathbf{I} \\ -\mathbf{M}_z^{-1} \mathbf{K}_{\Omega 0 z} & -\mathbf{M}_z^{-1} \mathbf{L}_z \end{bmatrix}$	
$\mathbf{A}_{\Omega 1}$	$\begin{bmatrix} \mathbf{0} & \mathbf{0} \\ -\mathbf{M}_{xy}^{-1} \mathbf{H}_{xy} & -\mathbf{M}_{xy}^{-1} \mathbf{G}_{xy} \end{bmatrix}$	$[\mathbf{0}]$	
$\mathbf{A}_{\Omega 2}$	$\begin{bmatrix} \mathbf{0} & \mathbf{0} \\ -\mathbf{M}_{xy}^{-1} \mathbf{K}_{\Omega 2 xy} & \mathbf{0} \end{bmatrix}$	$\begin{bmatrix} \mathbf{0} & \mathbf{0} \\ -\mathbf{M}_z^{-1} \mathbf{K}_{\Omega 2 z} & \mathbf{0} \end{bmatrix}$	
\mathbf{B}	$\begin{bmatrix} \mathbf{0} & \mathbf{0} & \mathbf{0} \\ \mathbf{I} & \mathbf{I} & \mathbf{S}_{ixy} \end{bmatrix}$	$\begin{bmatrix} \mathbf{0} & \mathbf{0} \\ \mathbf{I} & \mathbf{S}_{iz} \end{bmatrix}$	
$\mathbf{u}(t)$	$\begin{Bmatrix} \mathbf{f}_{sxy} \\ \mathbf{f}_{umb} \\ \mathbf{f}_{xy} \end{Bmatrix}$	$\begin{Bmatrix} \mathbf{f}_{sz} \\ \mathbf{f}_z \end{Bmatrix}$	
$\mathbf{y}(t)$	$\begin{Bmatrix} \mathbf{y}_{xy}(t) \\ \dot{\mathbf{y}}_{xy}(t) \end{Bmatrix}$	$\begin{Bmatrix} \mathbf{y}_z(t) \\ \dot{\mathbf{y}}_z(t) \end{Bmatrix}$	
\mathbf{C}	\mathbf{S}_{oxy}	\mathbf{S}_{oz}	
\mathbf{D}	$[\mathbf{0}]$	$[\mathbf{0}]$	

Table 12. State Space Representation variables.

4. Control design and results

The aim of this section is to explain the steps followed to perform the suspension control design. A conventional decentralized control strategy is illustrated with two nested loops, the inner for current control and the outer for the position. The detailed description of this strategy is followed by the exposition of an off-line electrical centering strategy which is used to equalize electrical parameters of the electromagnets on each actuation stage and allows to get a steady and balanced control action.

4.1. ActiveMagnetic Suspension Control

Figure 4 shows the classical control strategy for one axis AMB. The system is characterized with a nested control structure, where the inner loops describe the current loops used to achieve a direct actuator's effort drive (force) and the outer loop is used to compensate the rotor position error from the nominal air-gap. Generally, the same strategy is applied for each axis; so they are managed independently from each other and control is called decentralized. The driving of one axis is performed with two separate H-bridges. To exert a positive force on the rotor, current in the upper coil is increased by the control current while the current in the lower coil is decreased by control current and vice versa for negative forces. Also, to linearize the current to force characteristic of an electromagnet a constant bias current is applied to both coils respectively. Position control is performed by using five decentralized PID. The design and tuning of control laws parameters are well described in [1] and [2]. Here Bode diagram transfer function of position control law is reported (Figure11).

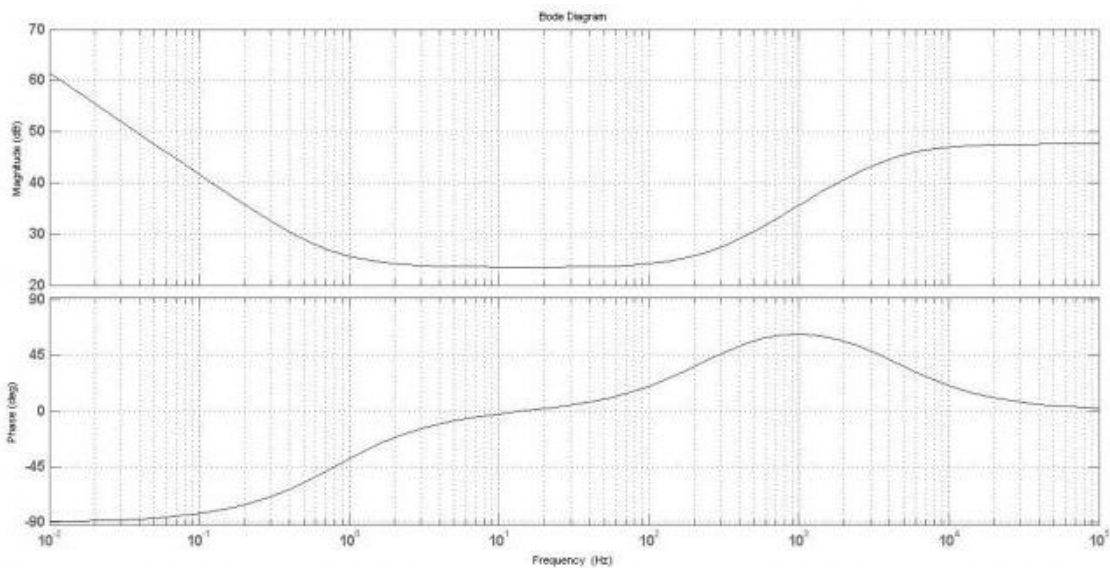


Figure 11. Control position Bode diagram.

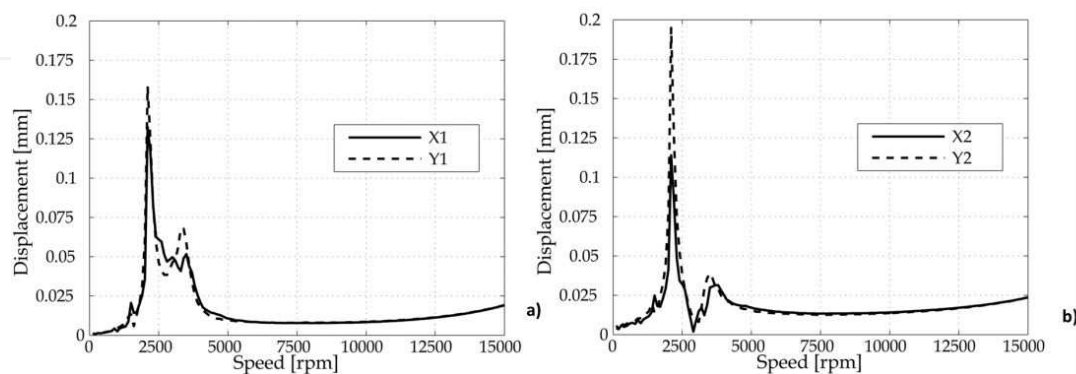


Figure 12. Unbalance response. a) Left actuation stage. b) Right actuation stage.

The experimental characterization has been performed by using classical tools of rotordynamic analysis: Unbalance responses (Figure 12), Waterfalls (Figure 13), orbital tube and orbital view (Figure 14, Figure 15). Theoretical notes on rotodynamic analysis can be found in [29].

4.2. Off-line Electrical Centering

Active Magnetic Bearings offer several technological advantages that make their use mandatory in some particular applications, typically when clean environment is required or maintenance is expensive or difficult to manage. On the other hand, the main drawbacks are mostly the costs, higher than classical ball bearings due to the introduction of sensors and electronic equipment, and the complexity in the design phases of electrical and electronics subsystems and control strategies.

One of the aspects where this difficulty is more evident is the centering of the rotating part respect to the stator and in particular to the sensors. Sensors are indeed designed to detect microns of displacements and little inaccuracies in measurements lead to bad working or to system instability in the worst cases.

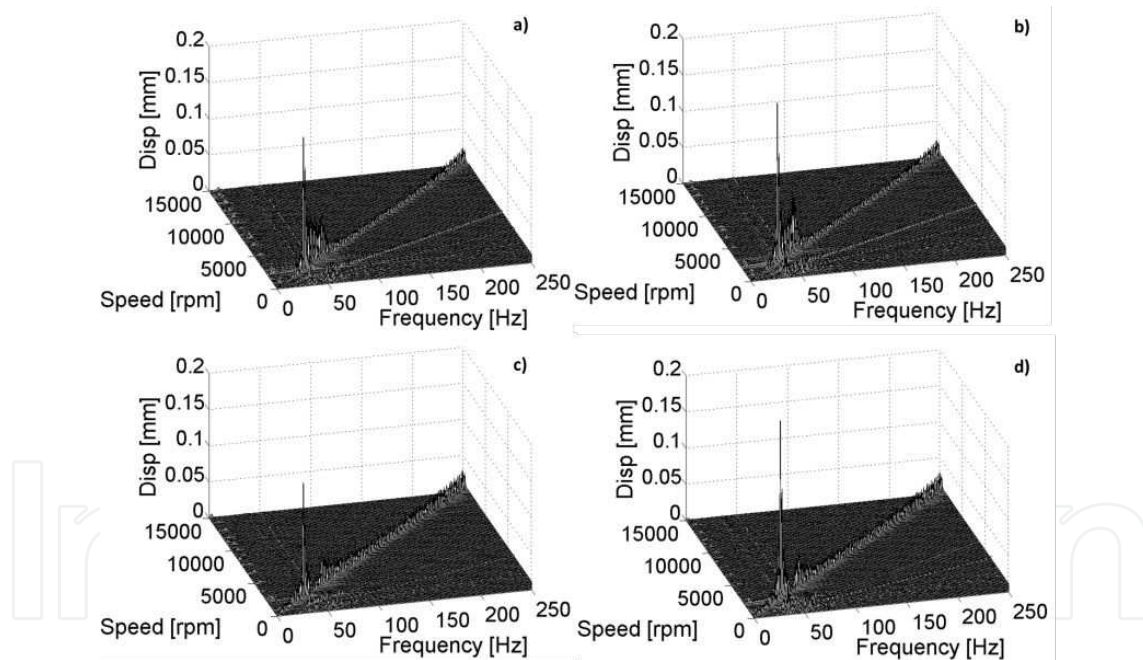


Figure 13. Waterfall plot. a) X1; b) Y1; c) X2; d) Y2.

The designer can choose to perform either a geometrical or an electrical centering, depending on the priorities of the application requirements. The first (Figure 16.a) consists in putting the rotor at the mechanical center neglecting the electrical differences in electromagnets coils parameters, inductance above all. The latter (Figure 16.b), on the contrary, leads to an equalization of electrical parameters, even if the rotor is not spinning around the geometrical center of the actuators.

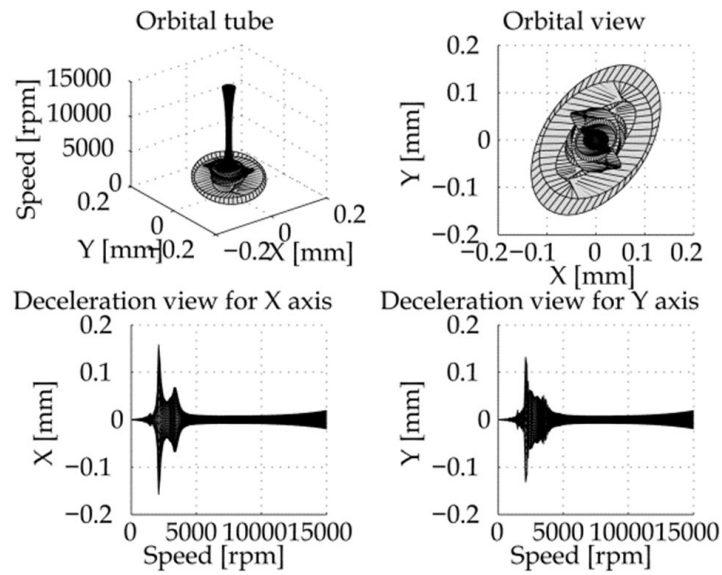


Figure 14. Orbital tube and orbital view representation on X1Y1 - plane. a) three dimensional view of the tube; b) Projection on the xy-plane; c) and d) projection on the Ω_x and Ω_y -planes.

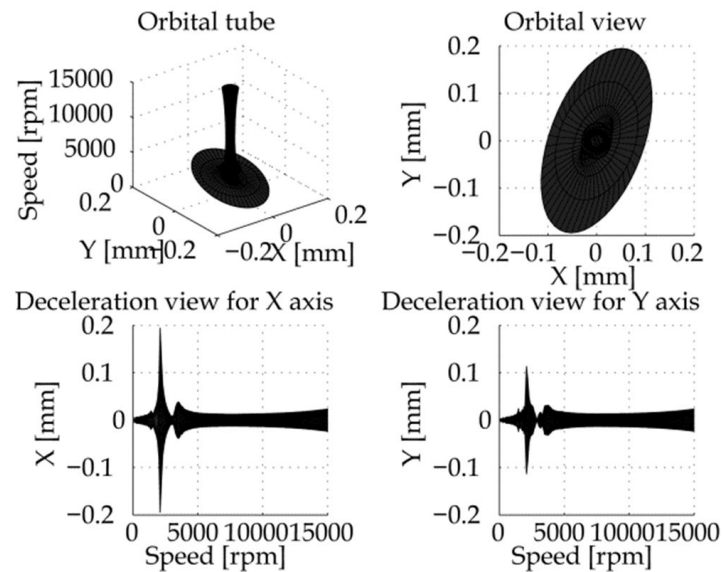


Figure 15. Orbital tube and orbital view on X2Y2 - plane. a) three dimensional view of the tube; b) Projection on the xy-plane; c) and d) projection on the Ω_x and Ω_y -planes.

In this section an off-line electrical centering technique is exposed. The goal is to make the rotor spins around a point which is not compulsorily coincident with the geometrical center of the actuators but grants the symmetry of the electrical parameters of them. It is well known that the inductance value of an electromagnet is depending on the distance between the ferromagnetic target (the rotor in this case) and the electromagnet itself.

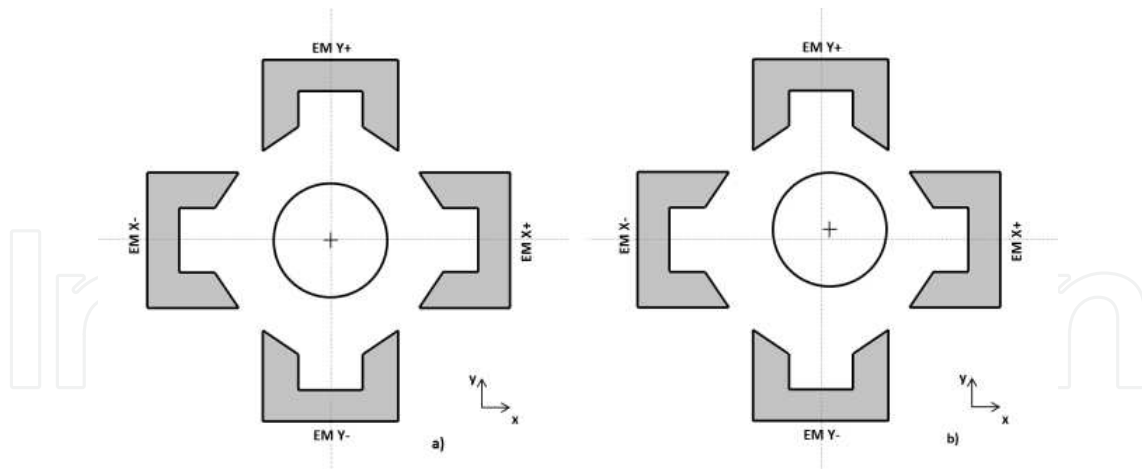


Figure 16. Mechanical centering (a) vs. Electrical centering (b).

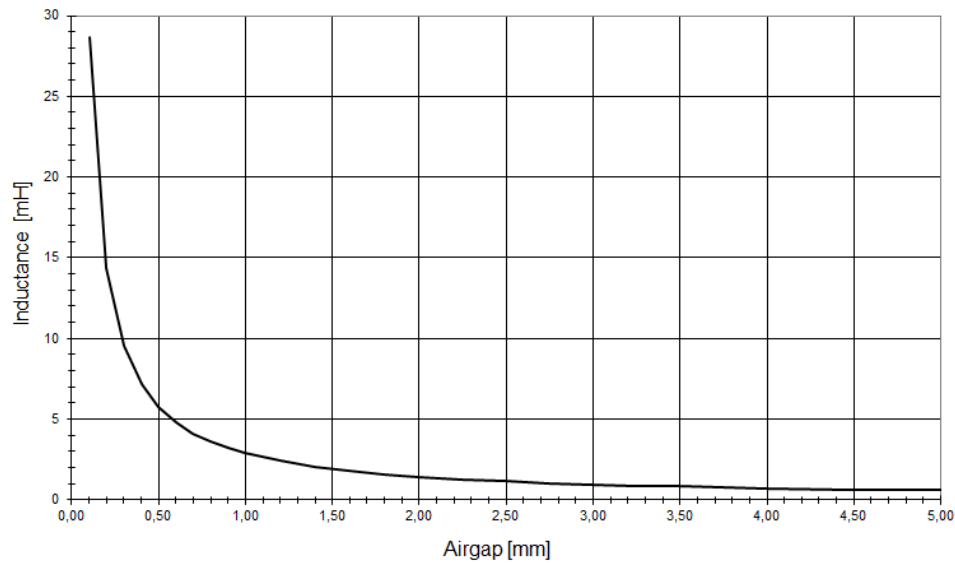


Figure 17. Inductance vs. Position.

This behavior is nonlinear as illustrated in Figure 17 and little variation of position and hence on inductance lead to big variation of actuator electrical pole and current control dynamics. Since the electrical dynamics of an electromagnet is depending on supply voltage, resistance and inductance values (Table 2) as in Eq. 17:

$$E = \frac{VDC}{R + Ls} \quad (9)$$

the electrical pole of the electromagnet is strictly dependent on the distance between the target and the actuator as reported in Figure 18. This issue has as consequence a different be-

havior of closed loop current control as illustrated in Figure 19 (a and b). It can be noticed that the same current control applied to the two opposite electromagnets of the same actuation axis without electrical centering generates two different closed loop responses. Few microns of Airgap generates differences of hundreds of Hertz on current control bandwidth.

Considering that this behavior is generated by a difference of inductance value of the two electromagnets, by acting on the position reference with offset corrections of the outer position control, the rotor can be set to spin around a point where electrical parameters are equalized and current loop bandwidths of both the electromagnets are the same (Figure 19 (c and d)). Further studies and research are being conducted on this strategy since this process can be performed in an on-line automatic routine with an adaptive technique, able to change the control parameters of the inner current loop while the Airgap is changing, i.e. when the rotor is oscillating.

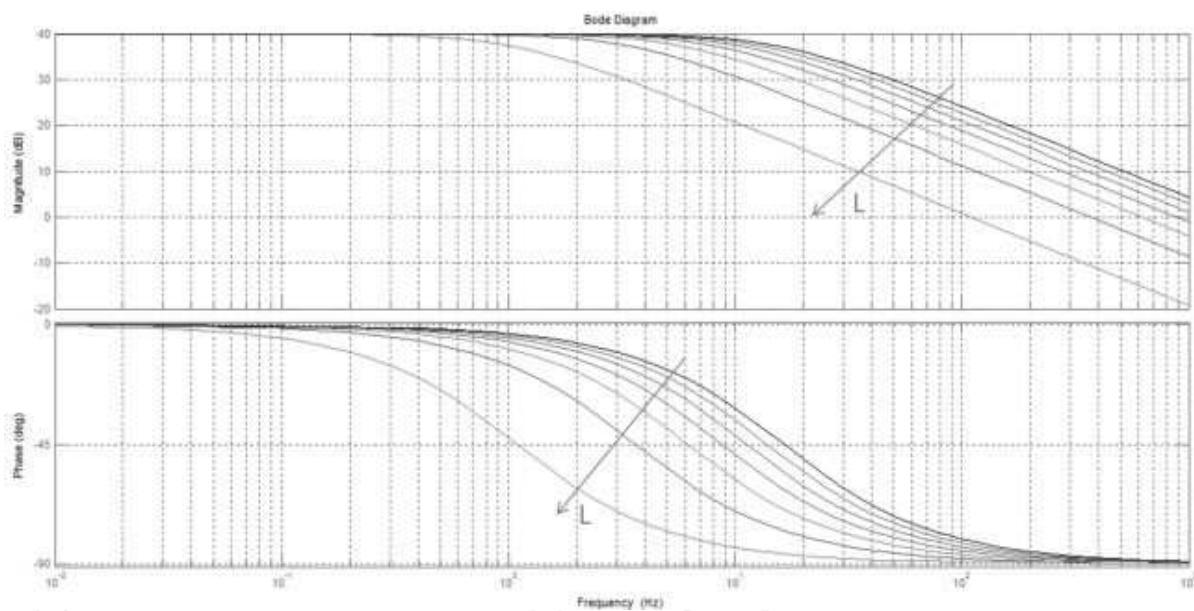


Figure 18. Electrical pole trend at varying of inductance value.

5. Conclusions

In this chapter the modeling, the design and the experimental tests phases of a rotor equipped with active magnetic bearings have been described. The description deals with rotordynamic aspects as well as electrical, electronic and control strategies subsystem. The control design of a standard decentralized SISO strategy and the details of an innovative off-line electrical centering technique have been exposed. Experimental results have been exposed highlighting mainly rotordynamics and control aspects.

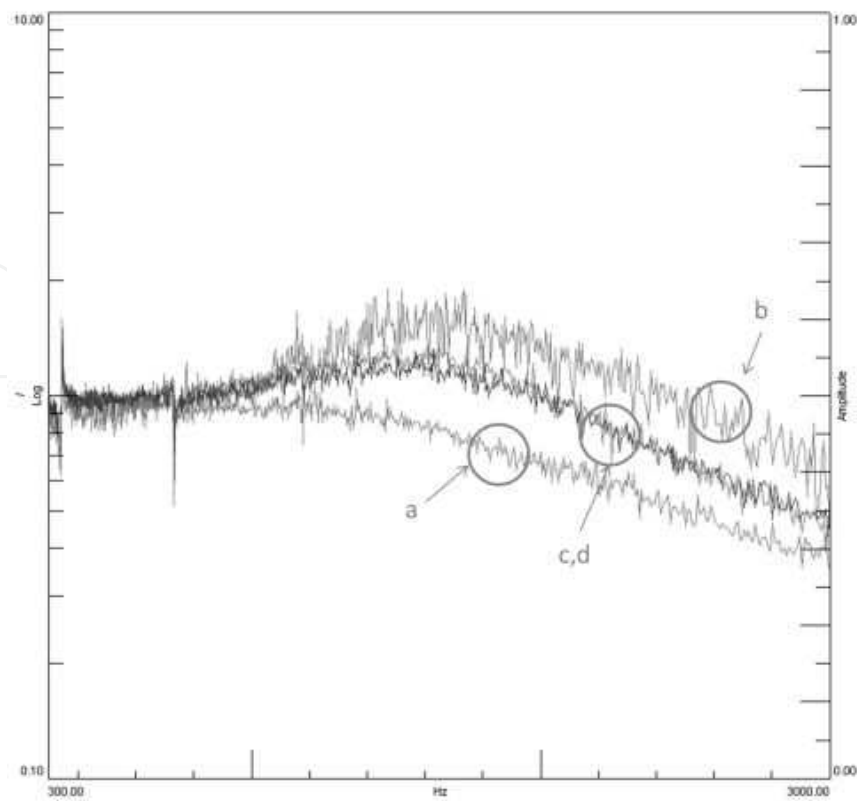


Figure 19. Electrical centering results. a) X- current loop Bode diagram before centering; b) X+ current loop Bode diagram before centering; c, d) X-/X+ current loop Bode diagrams after centering.

Author details

Andrea Tonoli, Angelo Bonfitto*, Mario Silvagni and Lester D. Suarez

*Address all correspondence to: angelo.bonfitto@polito.it

Mechanics Department, Mechatronics Laboratory – Politecnico di Torino, Italy

References

- [1] Bleuler, H., Cole, M., Keogh, P., Larssonneur, R., Maslen, E., Nordmann, R., Okada, Y., Schweitzer, G., & Traxler, A. (2009). *Magnetic Bearings Theory, Design, and Application to Rotating Machinery*, Springer, Berlin Heidelberg.
- [2] Chiba, A., Fukao, T., Ichikawa, O., Oshima, M., Takemoto, M., & Dorrell, D. G. (2005). *Magnetic Bearings and Bearingless drives*, Elsevier, Oxford.

- [3] Tonoli, A., Bonfitto, A., De Lépine, X., & Silvagni, M. (2009). Self-sensing Active Magnetic Dampers for vibration control. *Journal of Dynamic Systems, Measurement and Control*, 131.
- [4] Tonoli, A., Amati, N., Impinna, F., Detoni, J. G., Bleuler, H., & Sandtner, J. (2010). Dynamic Modeling and Experimental Validation of Axial Electrodynamic Bearings. Wuhan, China. *Proceedings of the 12th International Symposium on Magnetic Bearings*, 978-7-90050-306-0.
- [5] Genta, G., De Lépine, X., Impinna, F., Detoni, J. G., Amati, N., & Tonoli, A. (2009). Sensitivity Analysis of the Design Parameters of Electrodynamic Bearings. New Delhi, India. *IUTAM Symposium on Emerging Trends in Rotor Dynamics*, 287-296, DOI: 10.1007/978-94-007-0020-8, 1875-3507.
- [6] Bonfitto, A. (2012). *Active Magnetic Control of Rotors*, LAP LAMBERT Academic publishing AG & Co. KG, 978-3-84842-104-6.
- [7] Bosgiraud, T. (2008). Two Degrees of Freedom Miniaturized Gyroscope based on Active Magnetic Bearings. *PhD Thesis EPFL*, Lausanne, Switzerland.
- [8] Bleuler, H., Bonfitto, A., Tonoli, A., & Amati, N. (2010). Miniaturized gyroscope with bearingless configuration. In: *Twelfth International Symposium on Magnetic Bearings (ISMB12)*, Wuhan, China, August 22-25.
- [9] Schammas, A., Herzog, R., Buhler, P., & Bleuler, H. (2005). New results for self-sensing active magnetic bearings using modulation approach. *IEEE Trans. Contr. Syst. Tech.*, 13(4), 509-516.
- [10] Araki, Mizuno T., , K., & Bleuler, H. (1996). Stability analysis of self-sensing magnetic bearing controllers. *IEEE Trans. Contr. Syst. Tech.*, 4(5), 572-579.
- [11] Maslen, E. H., Montie, D. T., & Iwasaki, T. (2006). Robustness limitations in self-sensing magnetic bearings. *Journal of Dynamic Systems, Measurement and Control*, 128, 197-203.
- [12] Vischer, D., & Bleuler, H. (1990, 12-14 July). A new approach to sensorless and voltage controlled AMBs based on network theory concepts. Tokyo, Japan. *Second International Symposium on Magnetic bearings*, 301-306.
- [13] Vischer, D., & Bleuler, H. (1993). Self-sensing magnetic levitation. *IEEE Trans. on Magn.*, 29(2), 1276-1281.
- [14] Noh, M. D., & Maslen, E. H. (1997). Self-sensing magnetic bearings using parameter estimation. *IEEE Trans. Instr. Meas.*, 46(1), 45-50.
- [15] Betschon, F., & Knospe, C. R. (2001). Reducing magnetic bearing currents via gain scheduled adaptive control. *IEEE/ASME Transactions on Mechatronics*, 6(4), 437-443.
- [16] Lum, K. Y., Coppola, V. T., & Bernstein, D. S. (1996). Adaptive autocentering control for an active magnetic bearing supporting a rotor with unknown mass imbalance. *IEEE Trans. Contr. Syst. Technol.*, 4(5), 587-597.

- [17] Betschon, F., & Schob, R. (1998). On-line adapted vibration control. Cambridge, MA. *in Proc. 6th Int. Symp. Magnetic Bearings*, Mass. Inst. Technol., 362-371.
- [18] Hirata, M., Nonami, K., & Ohno, T. (1998). Robust control of a magnetic bearing system using constantly scaled H-infinity control. Cambridge, MA. *in Proc. 6th Int. Symp. Magnetic Bearings*, Mass. Inst. Technol., 713-722.
- [19] Kanemitsu, Y., Ohsawa, M., & Marui, E. (1994). Comparison of control laws for magnetic levitation. Zuerich. *in Fourth International Symposium on Magnetic Bearings, ETH*, 13-18.
- [20] Duan, G. R., & Howe, D. (2003). Robust magnetic bearing control via eigenstructure assignment dynamical compensation. *IEEE Trans. Contr. Syst. Technol.*, 11(2), 204-215.
- [21] Zhuravlyov, Y. N. (2002). On LQ-control of magnetic bearing. *IEEE Trans. Contr. Syst. Technol.*, 8, 344-355.
- [22] Steffani, H. F., Hofmann, W., & Cebulski, B. (1998). A controller for a magnetic bearing using the dynamic programming method of Bellman. Cambridge, MA. *in Proc. 6th Int. Symp. Magnetic Bearings*, Mass. Inst. Technol., 569-576.
- [23] Li, L. (1998). On-line tuning of AMB controllers using genetic algorithms. Cambridge, MA. *in Proc. 6th Int. Symp. Magnetic Bearings*, Mass. Inst. Technol., 372-382.
- [24] Hung, J. Y. (1995). Magnetic bearing control using fuzzy logic. *IEEE Trans. Ind. Appl. cat.*, 31, 1492-1497.
- [25] Lindlau, J. D., & Knospe, C. R. (2002). Feedback linearization of an active magnetic bearing with voltage control. *IEEE Trans. Contr. Syst. Technol.*, 10, 21-30.
- [26] Youcef-Toumi, K., & Reddy, S. (1992). Dynamic analysis and control of high speed and high precision active magnetic bearings. *ASME J. Dyn. Syst., Meas., Contr.*, 114, 623-633.
- [27] Mizuno, T. (2001). Analysis on the fundamental properties of active magnetic bearing control systems by a transfer function approach. *JSME Int. J. Series C. Mech. Syst. Mach. Elements Manufact.*, 44, 367-373.
- [28] Losch, F., Gahler, C., & Herzog, R. (1998, Aug. 5-7). synthesis controller design for a 3 MW pump running in AMBs. Cambridge, MA. *in Proc. 6th Int. Symp. Magnetic Bearings*, Mass. Inst. Technol., 415-428.
- [29] Genta, G. (2005). *Dynamics of Rotating Systems*, Springer, New York, 1-658, 978-0-38720-936-4.

